*Proceedings of Lunar and Planetary Science, Volume 21,* pp. 473-489
Lunar and Planetary Institute, Houston, 1991



# A Search for Spectral Units on the Uranian Satellites Using Color Ratio Images

**J. F. Bell III[1] and T. B. McCord**

***Planetary Geosciences Division, University of Hawaii, Honolulu, HI 96822***

We have analyzed 20 multispectral sets of calibrated, coregistered Voyager 2 images of the uranian satellites in an effort to identify spectrally (and thus possibly compositionally) distinct surface units and to associate these units with specific endogenic or exogenic surface processes. Morphologic unit mapping based on the initial work of Smith et al. (1986) has identified several regions on each satellite where significant spectral/compositional diversity could be expected. Color ratio images indicate that several of the satellites' surfaces exhibit significant color (as well as albedo) heterogeneity, and the majority of this heterogeneity is associated with impact craters. Oberon exhibits the highest degree of color variability, and we confirm the discovery by Helfenstein et al. (1990a) of a significant leading/trailing hemisphere color asymmetry. Titania and Ariel also show measurable impact-associated color variability, and we report on the possible existence of a hemispherical color asymmetry similar to Oberon's for Titania. Miranda (surprisingly) and Umbriel are very spectrally homogeneous. Several mechanisms for the origin of the color variability are discussed, including the possibility of an outer solar system analog to lunar vitrification darkening/reddening.

## 1. INTRODUCTION AND BACKGROUND

Visible (VIS) and near-infrared (NIR) disk-integrated spectral reflectance measurements have been obtained of the uranian satellites for several decades (e.g., *Harris,* 1961; *Johnson et al.,* 1978; *Reitsema et al.,* 1978; *Bell et al.,* 1979; *Cruikshank,* 1980; *Cruikshank and Brown,* 1981; *Soifer et al.,* 1981; *Brown,* 1983; *Brown and Clark,* 1984). Due to the faintness of these objects and their close proximity to Uranus, only disk-integrated spectra could be obtained. These spectra revealed diagnostic water-ice absorptions for each of the major uranian satellites (*Cruikshank,* 1980; *Cruikshank and Brown,* 1981; *Brown and Clark,* 1984). Data of *Brown* (1983) confirmed the presence of a dark, spectrally bland component on/in the water-ice surfaces of the satellites, but attempts to match the observed spectra with additive reflectance mixtures of fine-grained water-frost and various dark components failed to define, beyond broad limits, the composition of the dark component or its dominant mode of dispersal.

Voyager 2 images provide our only detailed look at surface features on these satellites, although only the southern hemispheres were visible and spatial resolution typically does not exceed 1 km/pixel (*Smith et al.,* 1986; *Davies et al.,* 1987; see also U.S. Geological Survey Map I-1920, 1988). Voyager imaging and spectral coverage was limited to visible wavelengths (Fig. 1). These images showed evidence for large-scale tectonism and resurfacing on all the satellites (*Smith et al.,* 1986; *Plescia,* 1987; *Strom,* 1987; *Helfenstein et al.,* 1989b, 1990b; *Croft and Soderblom,* 1990).

*Smith et al.* (1986), *Veverka et al.* (1987), and *Buratti et al.* (1990) have compiled disk-averaged albedos at the six central wavelengths of the narrow-angle camera filters for the five main uranian satellites (Fig. 2). *Smith et al.* (1986) and *Veverka et al.* (1987) obtained similar results, indicating that the bulk spectral behavior of the satellites is gray to very slightly red in the visible. *Buratti et al.* (1990) used recently improved groundbased calibration factors and found a greater spread in bulk spectral properties and also found Titania to be slightly redder than Oberon by a few percent. The satellites' disk-averaged albedos are roughly similar to those of Saturn's Phoebe or many C-type asteroids, but are not as red as D-type asteroids or the dark material of Iapetus (*Smith et al.,* 1986). Initial analysis of selected bright and dark areas on the surfaces of several satellites by these authors did not reveal any significant spectral variability. This was not surprising, though, in light of the fact that the spectra of most candidate dark materials and of water-ice are relatively flat in this wavelength region.

Disk-integrated photometric parameters for the uranian satellites have more recently been determined using both Hapke models (*Veverka et al.,* 1987; *Helfenstein et al.,* 1988; *Buratti et al.,* 1990) and Minnaert models (*Veverka et al.,* 1989; *Hillier et al.,* 1989). The satellites were found to exhibit a range of disk-integrated albedos, phase coefficients, regolith compaction parameters, and large-scale roughness that indicates a good deal of bulk geologic and/or compositional heterogeneity in the uranian system.

Recent disk-resolved photometric studies have indeed revealed a significant degree of inter- and intrasatellite spectral and/or compositional heterogeneity. Bright and dark surface units on Titania were studied by *Thomas et al.* (1987), who found the regolith to be somewhat less compacted in bright regions associated with impact craters and ejecta. *Helfenstein et al.* (1989b) have found evidence for a global pattern of low-contrast albedo markings on Umbriel, which they interpret as evidence of early volcanic/tectonic resurfacing events. *Hillier et al.* (1989) have done a detailed examination of surface units on Miranda and found the surface to be surprisingly homogeneous in color, despite large albedo contrasts and

[1]Currently at Geological Remote Sensing Lab, Mail Code AJ-20, University of Washington, Seattle, WA 98195

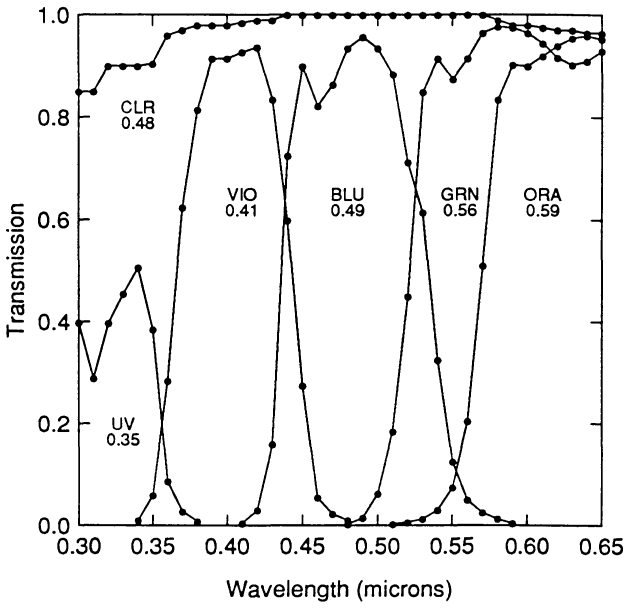


**Fig. 1.** Voyager 2 narrow angle camera filter transmission functions as given in *Danielson et al.* (1981). These filter abbreviations and effective center wavelengths ($\lambda_{eff}$) are used throughout the text.

ample evidence for resurfacing events and extensive tectonism. Oberon, with its bright, measurably bluer crater ray materials, seems to exhibit the greatest degree of surface color heterogeneity of all the satellites (*Helfenstein et al.,* 1989a, 1990a,b; *Bell,* 1990).

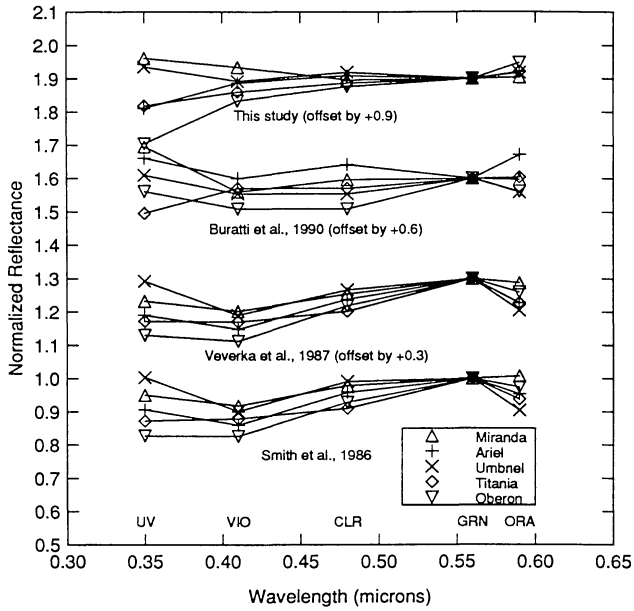


**Fig. 2.** Disk-averaged spectra for the major uranian satellites as derived by *Smith et al.* (1986), *Veverka et al.* (1987), *Buratti et al.* (1990), and this study. The data are normalized to unity at the GRN filter and each group is offset for clarity.

Our goals for this research were to expand on these previous efforts and identify spectrally heterogeneous regions on the uranian satellites, relating these regions to specific morphologic features and to specific exogenic or endogenic processes. In this paper we first briefly discuss the dataset and calibration/reduction procedures, then outline our procedure for identifying the best "candidate" regions on the satellites with the greatest potential for spectral heterogeneity. Next, pseudospectra and color ratio images are presented, showing contiguous spatial variability of surface spectral properties on several of the satellites. Finally, the implications of the various spectral units on each of the satellites are discussed as they relate to surface composition and regolith evolution and modification.

## 2. DATASET AND CALIBRATION/REDUCTION

Raw, uncalibrated Uranus satellite imaging data were obtained from the National Space Sciences Data Center/ Planetary Data System CDROM dataset. These raw images were processed using the USGS Planetary Image Cartography System (PICS) and University of Washington Image and Spectral Processing (WISP) software. Geometric and radiometric correction parameters were updated using the most recent PICS/JPL geometric calibration files. This allowed automatic reseaux location and removal, "de-spiking" of spurious pixels, dark current subtraction, and flatfielding within PICS. The images at this stage represent geometric albedo or I/F (where I is the intensity at each pixel and $\pi$F is the incident solar flux at 19.1 AU) and must still be radiometrically corrected using "calibration factors." These calibration factors are constantly refined and updated multiplicative constants applied to each filter image in an attempt to correlate Voyager data with inflight camera calibration and groundbased telescopic spectral studies of the satellites (*Danielson et al.,* 1981; T. V. Johnson et al., unpublished data, 1986). Values used here are: UV, $1.186 \pm 0.08$; VIO, $1.125 \pm 0.04$; BLU, 1.000 (by definition); CLR, $1.023 \pm 0.05$; GRN, $0.926 \pm 0.03$; ORA, $0.935 \pm 0.02$. The large error associated with several of these calibration factors (especially the ultraviolet or UV value), uncertainties in pointing geometry and camera/filter calibration, plus frequently low S/N associated with the low albedo of these objects all combine to yield a photometric uncertainty of up to ±5% (up to ±10% for the UV), although relative photometry between filters is somewhat better, with a maximum uncertainty of ±3% (*Danielson et al.,* 1981; *Buratti et al.,* 1990).

Calibrated single-filter images were coregistered either by a simple x,y transformation or by bilinear tiepoint fitting when there was significant spacecraft/satellite parallax. No corrections for differences in photometric geometry between images have been performed, and the spectra discussed here have been scaled to unity at the GRN filter ($\lambda_{eff} = 0.56$ $\mu$m).

Through this process, 20 sets of up to 6 color-calibrated, coregistered images of the 5 major satellites at band centers of 0.35-0.59 $\mu$m were generated (Table 1). These represent all those images for which the above calibration exercise could be carried out using available software and spacecraft pointing data. The color image sets were treated as "image cubes";

TABLE 1. Voyager 2 Uranus satellites color image groups.

| Satellite | Group # | FDS Range | $\alpha$ | Colors* | Size† | Comments |
|---|---|---|---|---|---|---|
| Miranda | 1 | 26844.09-26844.15 | 16° | 4 | 370 | High spatial resolution (2 km) |
| | 2 | 26796.35-26796.53 | 15° | 4 | 25 | Poor spatial resolution |
| | 3 | 26783.16-26783.46 | 18° | 6 | 18 | Best spectral resolution |
| Ariel | 1 | 26843.38-26843.44 | 32° | 4 | 700 | Only 75% of disk imaged |
| | 2 | 26797.28-26797.46 | 21° | 4 | 50 | Poor spatial resolution |
| | 3 | 26790.29-26790.59 | 19° | 5 | 45 | Poor spatial resolution |
| | 4 | 26780.48-26781.18 | 16° | 6 | 40 | Best spectral resolution |
| Umbriel | 1 | 26825.51-26826.03 | 31° | 3 | 120 | Best spatial resolution |
| | 2 | 26797.04-26797.22 | 12° | 4 | 55 | Worst spatial resolution |
| | 3 | 26787.45-26788.15 | 10° | 6 | 40 | Best spectral resolution |
| | 4 | 26778.54-26779.42 | 11° | 5 | 35 | Poor S/N |
| Titania | 1 | 26836.49-26836.55 | 34° | 3 | 345 | Best spatial resolution |
| | 2 | 26825.06-26825.24 | 9° | 4 | 180 | Best $\alpha$ coverage images |
| | 3 | 26820.28-26820.46 | 4° | 4 | 150 | Best $\alpha$ coverage images |
| | 4 | 26818.31-26818.49 | 2.5° | 4 | 145 | Best $\alpha$ coverage images |
| | 5 | 26816.58-26817.16 | 1.5° | 4 | 135 | Best $\alpha$ coverage images |
| | 6 | 26814.59-26815.17 | 0.75° | 4 | 125 | Lowest phase angle data |
| | 7 | 26776.22-26776.32 | 12° | 5 | 55 | Best spectral resolution |
| Oberon | 1 | 26836.25-26836.29 | 39° | 3 | 250 | Best spatial resolution |
| | 2 | 26787.05-26787.35 | 19° | 6 | 60 | Best spectral resolution |

* Denotes total number of filter images in that group, including CLR.
† Denotes total apparent diameter of satellite in pixels within each 800 × 800 frame.

spectra of various regions on the satellites were extracted and color ratios and two-dimensional histograms were generated in an attempt to take advantage of the excellent spatial resolution within these multispectral data.

## 3. MORPHOLOGIC UNIT MAPS

Numerous regions of the satellites' surfaces were "tagged" for special attention in the color ratio images by first creating a detailed set of morphologic unit maps. The best spatial resolution color images for each satellite were chosen for photogeologic mapping. These images do not, in several cases, correspond to the closest approach images (acquired for the CLR filter only on the cases of Ariel, Miranda, and Titania) but do exhibit comparable spatial resolution. On the sketch maps presented in Figs. 3-7, the various mapped units were chosen mostly on the basis of albedo and structural trend boundaries (following the original unit definitions of *Smith et al.,* 1986 and in general agreement with the recent work of *Croft and Soderblom,* 1990), thus they do not necessarily represent compositional units. Regardless, we feel that the units outlined here highlight the most likely regions on the satellites where compositional differences *could* arise, either as a result of exogenic (large impact craters or basins) or endogenic (tectonism and/or large-scale resurfacing) processes. Our concentration has focused on the following regions.

### 3.1. Miranda

The imaged part of the southern hemisphere of Miranda (Fig. 3) is dominated by two large, roughly ellipsoidal shaped "coronae" several hundred kilometers in extent. These banded terrains have generally darker albedo than the surrounding cratered plains, as well as several inner "islands" of lighter plains-type material (*Smith et al.,* 1986; *Croft and Soderblom,* 1990). The most noteworthy of these is the bright chevron-shaped feature within Inverness Corona (labeled B in Fig. 3b). The origin of the coronae is unknown but may be related to extrusive cryovolcanism (*Smith et al.,* 1986; *Croft,* 1987; *Jankowski and Squyres,* 1988), large-scale impact and subsequent resurfacing (*Janes and Melosh,* 1988), Ganymede-like extensional cracks and grooves, disruption or reaccretion of the satellite (*Smith et al.,* 1982), or embryonic differentiation (*Johnson et al.,* 1987). All these models predict possible compositional variability associated with the coronae. Other areas of possible compositional diversity include prominent impact craters that may excavate quite deep into Miranda's crust.

### 3.2. Ariel

The imaged area of Ariel (Fig. 4) is littered by small, bright impact craters and a system of complex smooth-floored troughs and ridges near the terminator. Higher-resolution images indicate that these graben may be tectonic/volcanic in origin, exhibiting medial grooves or ridges possibly indicative of extruded viscous materials (*Smith et al.,* 1986; *Jankowski and Squyres,* 1988). Bright craters and their extended ejecta deposits such as Melusine and Laica (labeled B and C in Fig. 4b) may also be regions of compositional variability.

1991LPSC...21..473B



(a)

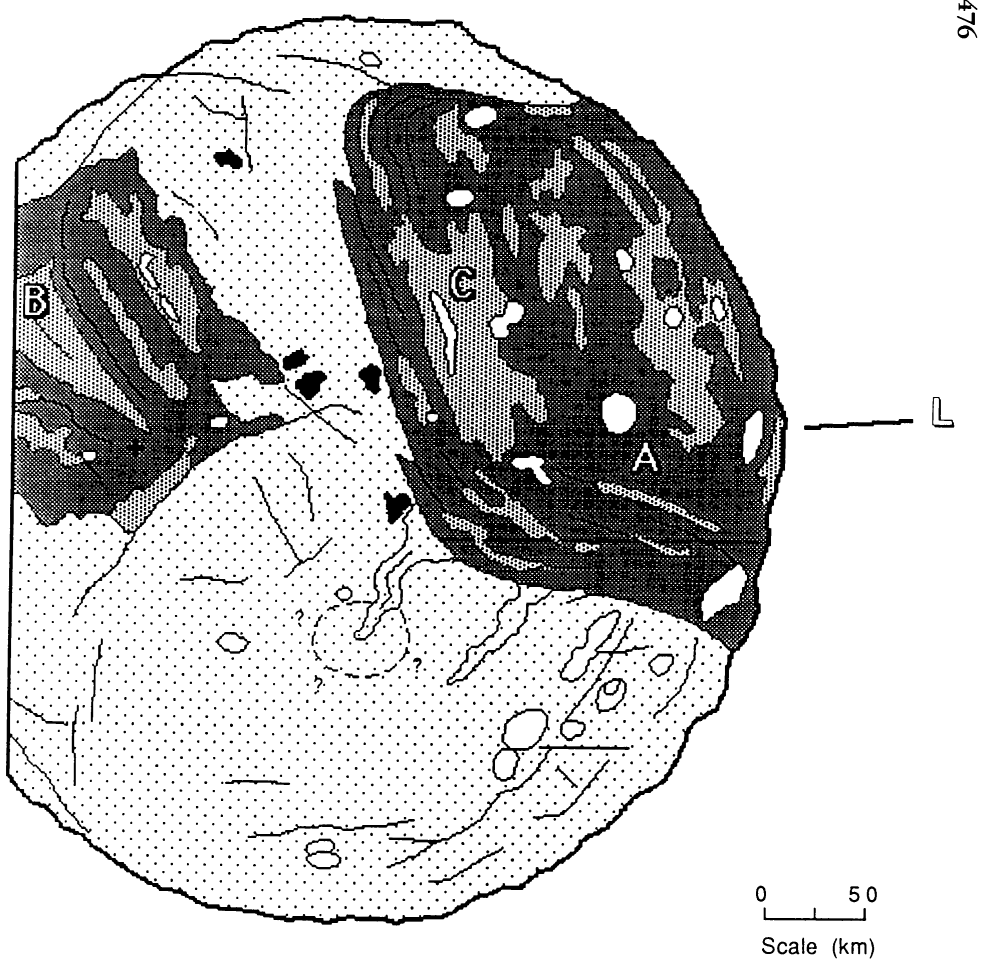


(b)

**Fig. 3.** **(a)** Highest spatial resolution color image of Miranda (VIO filter, $\lambda_{eff} = 0.56$ $\mu$m, FDS #26844.11). **(b)** Geomorphic sketch map of Miranda, based on the image in **(a)**, highlighting the most likely regions where compositional variability *could* arise. Mapping such as this for all the satellites is based on the original unit definitions of *Smith et al.* (1986). The cross indicates the south pole and the L indicates the central longitude of the leading hemisphere.

**Miranda Morphologic Units**

Map Key

- Heavily Cratered Terrain
- Dark Coronal Plains
- Light Coronal Plains
- Impact Crater/Ejecta, Light
- Impact Crater/Ejecta, Dark
- Major Lineations/Scarps

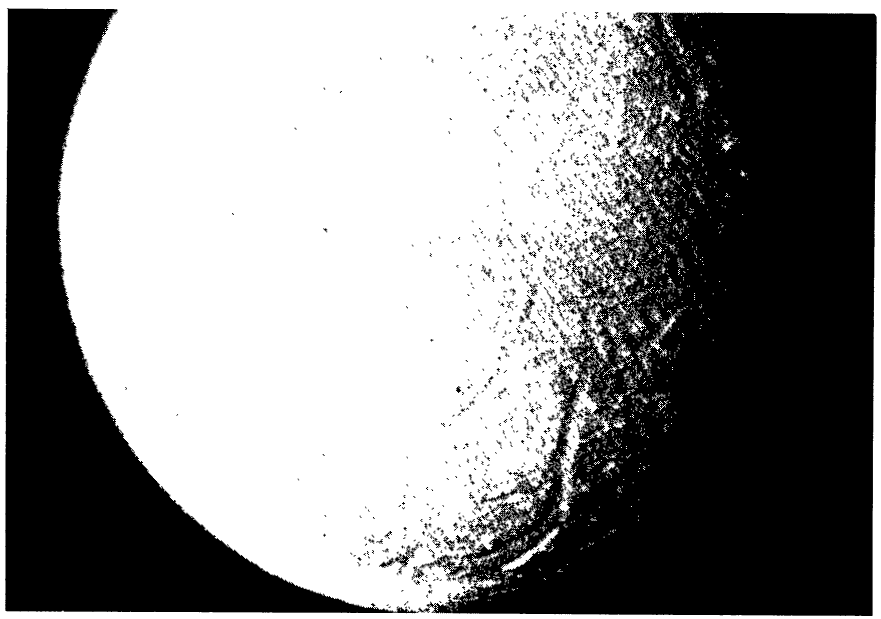

(a)

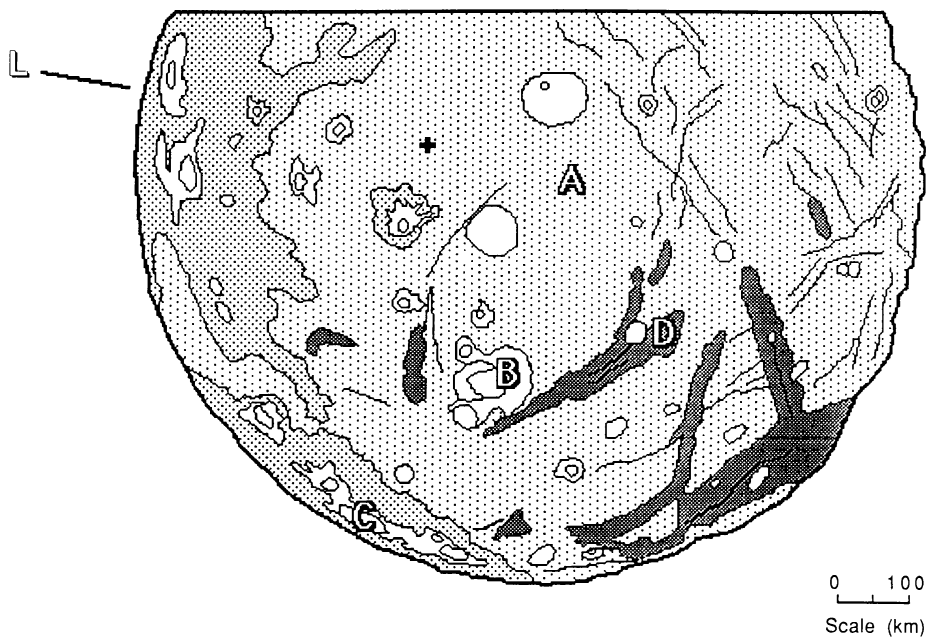


(b)

**Ariel Morphologic Units**

Map Key

- Heavily Cratered Terrain
- Impact Craters/Ejecta
- Extended Ejecta/Light Plains
- Smooth Floor/Flow Unit
- Major Lineations/Scarps

**Fig. 4.** **(a)** Highest spatial resolution color image of Ariel (GRN filter, $\lambda_{eff} = 0.56\ \mu m$, FDS #26843.42). **(b)** Geomorphic sketch map of Ariel. The cross indicates the south pole and the L indicates the central longitude of the leading hemisphere.

1991LPSC...21..473B



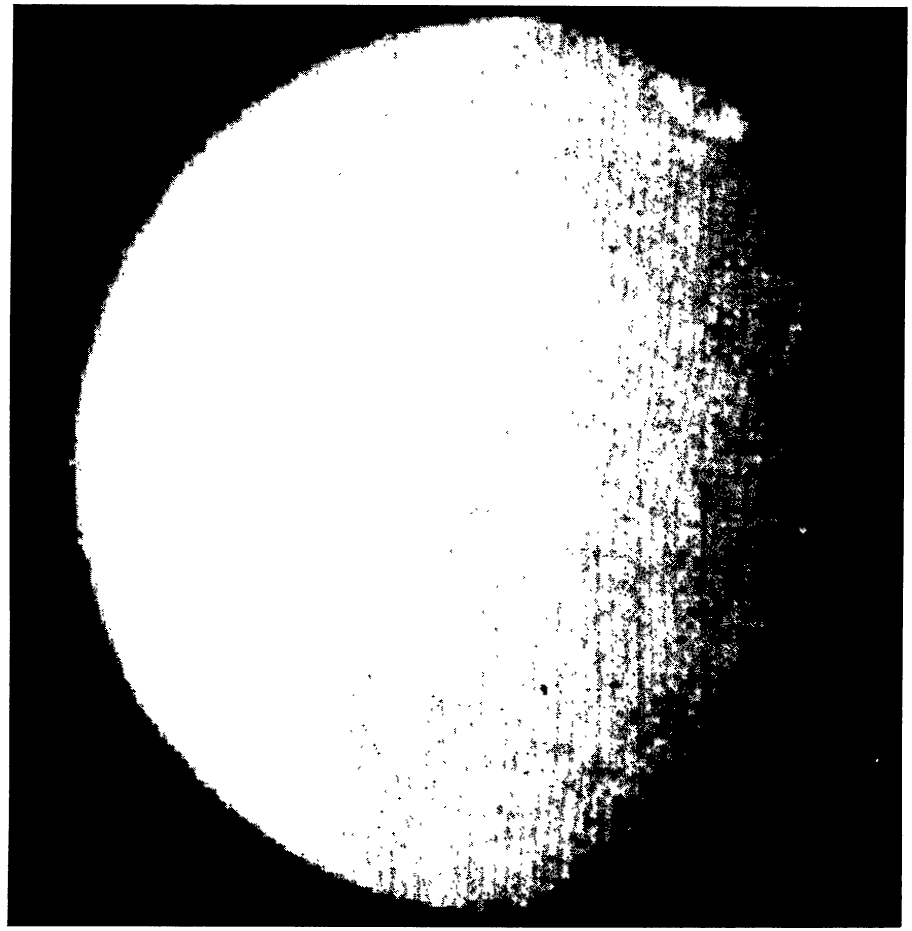

(a)

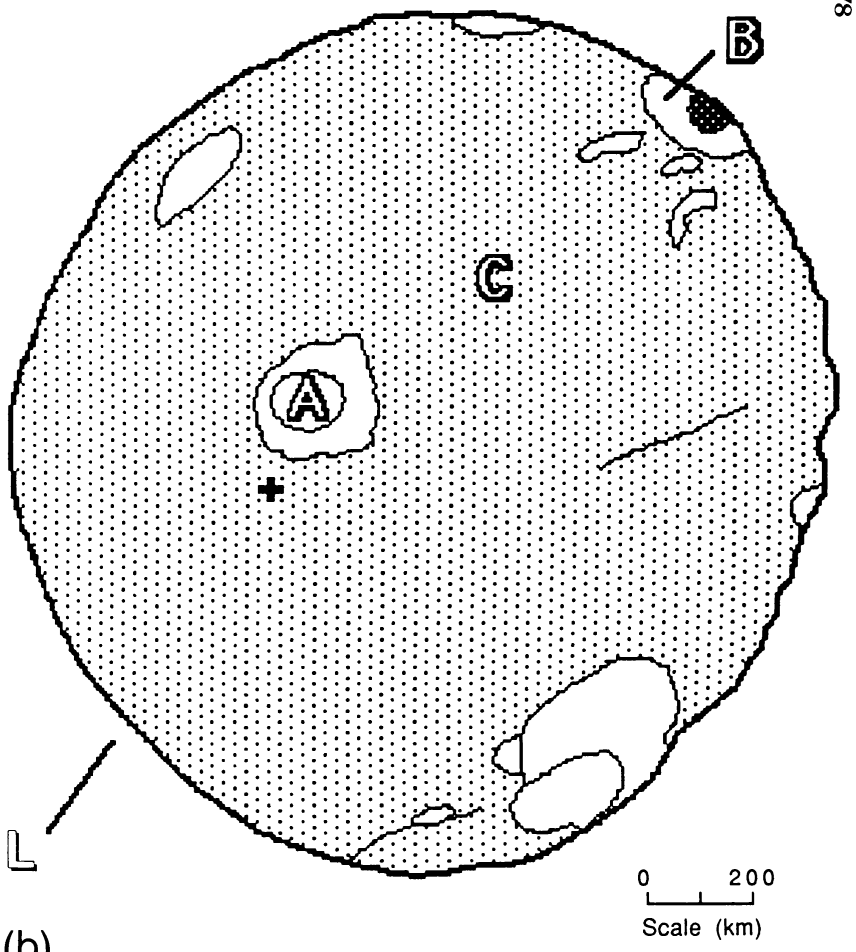


(b)

**Fig. 5.** **(a)** Highest spatial resolution color image of Umbriel (GRN filter, $\lambda_{eff} = 0.56$ $\mu$m, FDS #26826.03). **(b)** Geomorphic sketch map of Umbriel. The cross indicates the south pole and the L indicates the central longitude of the leading hemisphere.

**Umbriel Morphologic Units**

Map Key

- Heavily Cratered Terrain
- Impact Craters/Ejecta
- Dark Crater Floor Deposits
- Major Lineations/Scarps

1991LPSC...21..473B

(a)

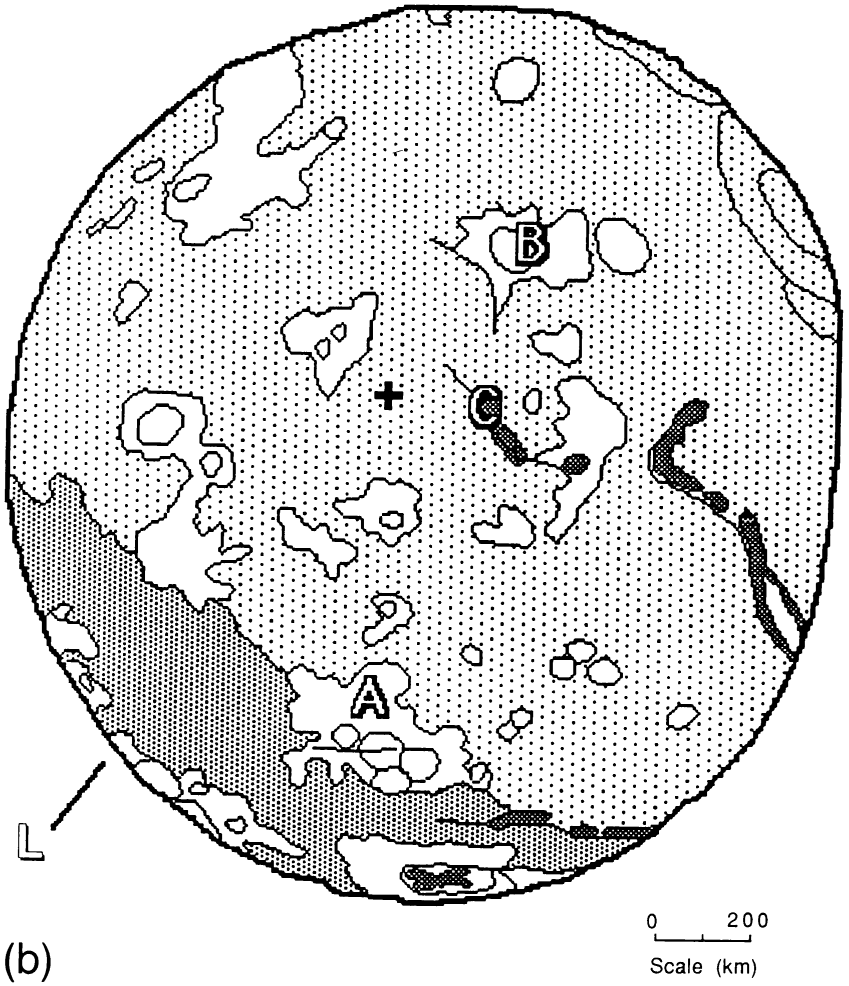


(b)

**Fig. 6.** **(a)** Highest spatial resolution color image of Titania (GRN filter, $\lambda_{eff} = 0.56\ \mu m$, FDS #26836.55). **(b)** Geomorphic sketch map of Titania. The cross indicates the south pole and the L indicates the central longitude of the leading hemisphere.

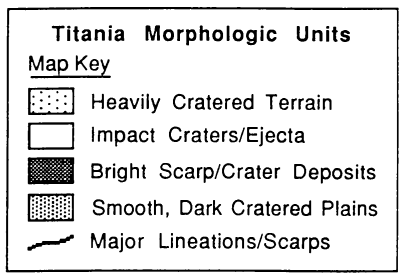

1991LPSC...21..473B



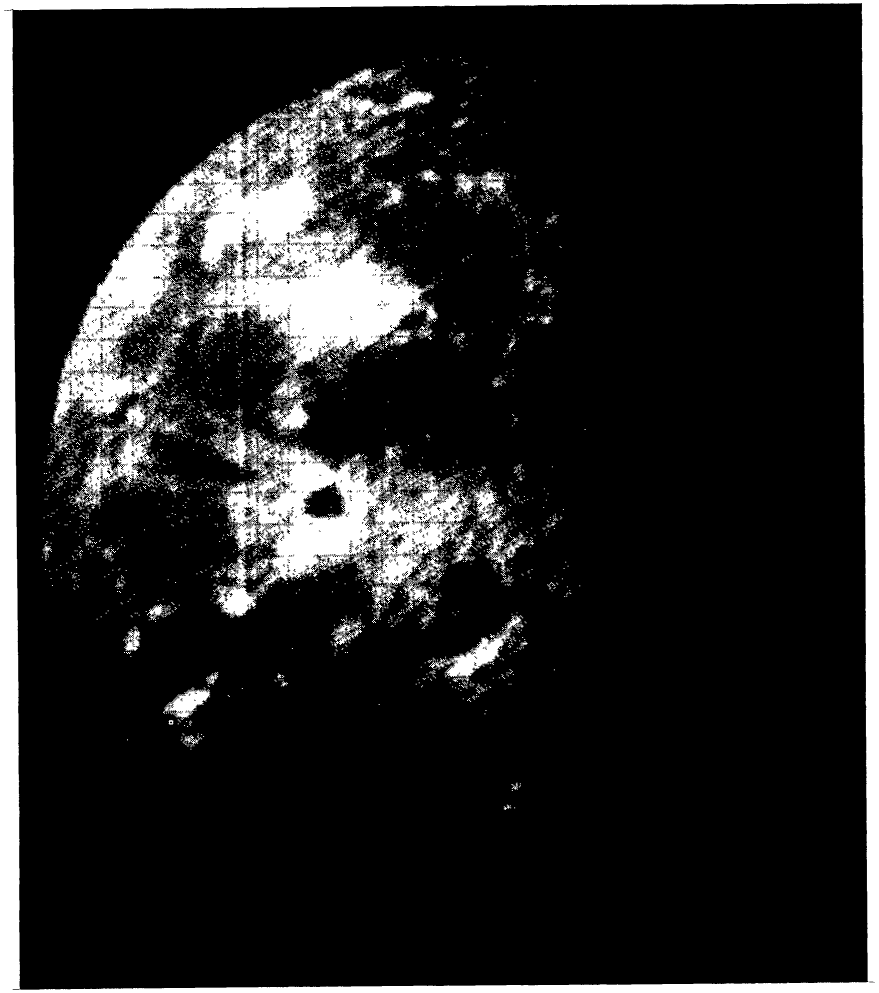

(a)

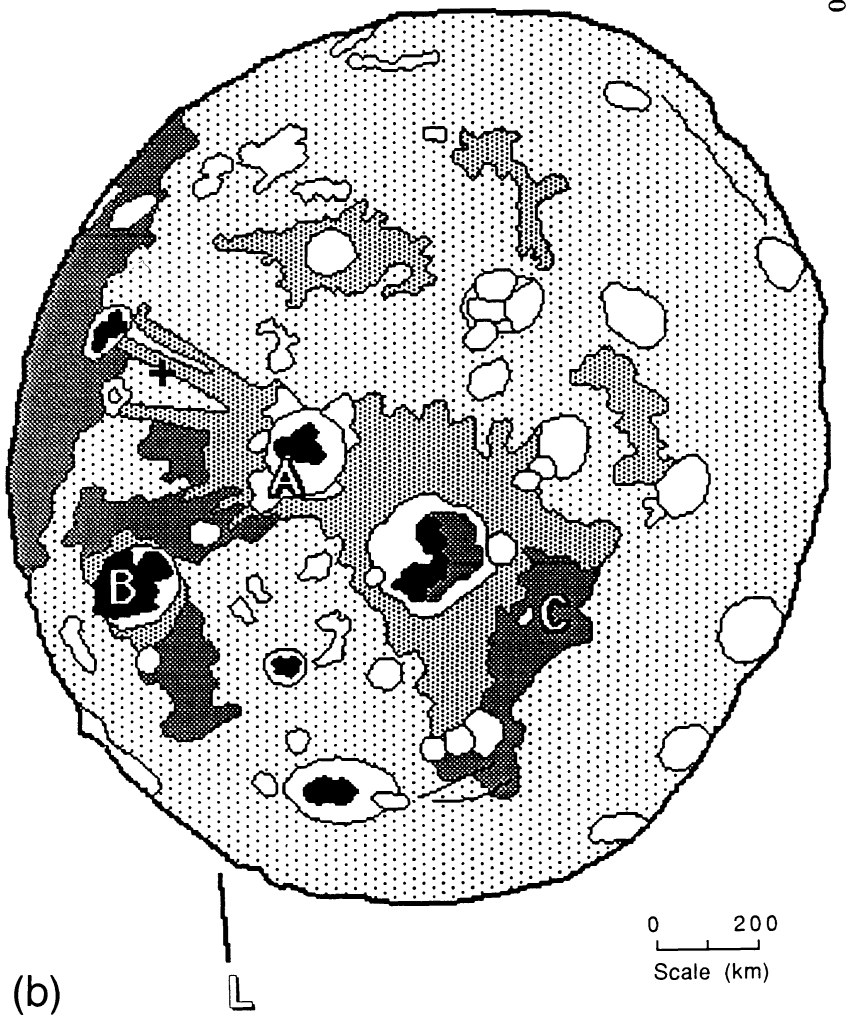


(b)

**Oberon Morphologic Units**

Map Key

- Heavily Cratered Terrain
- Impact Craters/Ejecta
- Dark Crater Floor Deposits
- Bright Extended Ejecta Blanket and Ray Materials
- Dark Extended Ejecta Blanket
- Major Lineations/Scarps

**Fig. 7.** **(a)** Highest spatial resolution color image of Oberon (GRN filter, $\lambda_{eff} = 0.56\ \mu m$, FDS #26836.29). **(b)** Geomorphic sketch map of Oberon. The cross indicates the south pole and the L indicates the central longitude of the leading hemisphere.

### 3.3. Umbriel

The southern hemisphere of Umbriel (Fig. 5) is dominated (90-95%) by an ancient, very dark, heavily cratered unit. The only albedo features that stand out in the color data and possibly excavate different materials are several bright craters along the equatorial terminator (Wunda and Vuver, labeled B in Fig. 5b) and a vaguely discernable crater near the south pole (labeled A).

### 3.4. Titania

Many large, smooth-floored impact craters and basins, as well as scarps such as Messina Chasmata (labeled C in Fig. 6b), indicate regions in Titania's southern hemisphere where surface composition may vary (Fig. 6). Smoother, darker plains regions evident in the color data but best seen in high-pass filtered images (*Smith et al.,* 1986; *Plescia,* 1987) near the crater Ursula (adjacent to the crater labeled A) also represent possible heterogeneous regions, as do other small, bright craters such as Jessica (labeled B).

### 3.5. Oberon

The southern hemisphere of Oberon (Fig. 7) exhibits a high degree of albedo contrast and several potentially distinguishable compositional units. Most interesting of these are dark crater floor material seen within the craters Hamlet and Othello (*Smith et al.,* 1986; labeled B in Fig. 7b) and also extended ejecta blankets and ray material associated with these same craters (labeled A and C). Other smaller, bright craters could possibly excavate spectrally distinct materials.

## 4. SATELLITE AND UNIT SPECTRA

Pseudospectra were extracted from the multispectral images for the whole disk of each satellite and for selected units based on the photogeologic mapping discussed above. The phase angle ($\alpha$) often varied considerably for different groups of images for each satellite, resulting in a spectral offset. This effect was alleviated somewhat by scaling the data to 1 at the GRN filter ($\lambda_{eff} = 0.56\ \mu m$) and relies on the assumption that phase angle effects are not significantly wavelength-dependent across this spectral range (*Veverka et al.,* 1987; however, see also *Buratti et al.,* 1990). Our whole-disk spectra are presented in Fig. 2. The only significant difference between these and previous whole-disk data (*Smith et al.,* 1986; *Veverka et al.,* 1987; *Buratti et al.,* 1990) is in the UV filter, which has the lowest S/N and the most uncertain calibration factor. Other small differences between these datasets fall well within the errors associated with the calibration factors and the small number statistics of the data in several filters (for example, the only BLU data for Miranda were obtained when the satellite was only 18 pixels in diameter).

In addition, we attempted to produce pseudospectra of individual surface units on the satellites. This has proved to be extremely difficult due to several factors. First, the highest spatial resolution images were obtained in the fewest colors and vice versa. Individual unit boundaries are often impossible to locate at lower spatial resolution (cf. Figs. 10b, 12b, and 13b), and thus only limited color information can be obtained for the most interesting regions on the satellites. Second, the rather large errors associated with the filter calibration factors (discussed above), misregistration effects, and phase/color variations all introduce additional uncertainty in the spectra, and this uncertainty is well above the level of spectral variation seen on these bodies. Although individual unit spectra can be extracted and intercompared after carrying out our low-level calibration exercise (section 2), the large error bars associated with these measurements make the interpretation of such spectra questionable. Further efforts concentrating on more rigorous image coregistration, a detailed analysis of the effects of color variations with phase angle, and a more complete assessment of the total error associated with each pixel in each color is needed before such data can be presented (see, for example, *Hillier et al.,* 1989; *Helfenstein et al.,* 1990a,b).

## 5. COLOR RATIO IMAGES

The multispectral imaging data acquired and calibrated as described above were normalized by adding together the flux for each pixel at all wavelengths sampled and dividing each pixel by that sum. This effectively removes the albedo (spectral offset) information from each image, and remaining light/dark variations are related to changes in spectral shape only. From these normalized data, color ratio images and two-dimensional histograms were obtained. For this simplistic analysis, the data were not map projected nor did we correct for the effects of photometric geometry or parallax.

### 5.1. Miranda

The Miranda GRN/VIO ratio image (Fig. 8) suffers from some misregistration problems near the terminator (very bright regions), but elsewhere is informative. The reddest, most anomalous surface units are associated with small (15 km) bright impact craters in Inverness and Arden Coronae that exhibit GRN/VIO = $1.12 \pm 0.05$ to $1.18 \pm 0.09$. The lowest ratio region associated with the uniform heavily cratered terrain has GRN/VIO = $0.95 \pm 0.04$, while higher ratio regions that outline the major coronae have GRN/VIO = $0.97 \pm 0.04$ to $1.00 \pm 0.06$. It could be argued that since these variations are only slightly out of the noise, they may not really be indicating true color heterogeneity. In fact, some support for this can be seen in the GRN vs. VIO two-dimensional histogram of Fig. 9a, which shows a high correlation of the reflectance values at these two wavelengths (85% of the variance between these two images is along this major trend). However, by plotting the GRN/VIO ratio vs. VIO reflectance as in Fig. 9b, most of this high correlation is removed. The resulting data cloud is still rather compact, but subtle variations between the color of the high albedo (less red) and intermediate albedo (more red) terrains can be seen (Fig. 9b). The observed spatial association of color variability in the ratio image with known morphologic units as mapped in Fig. 3b could also be an indicator of slight misregistration or shadowing variations associated with large changes in topography (ridges and troughs). It is interesting to note that the bright chevron feature inside Inverness Corona has nearly the *same* ratio value as the heavily cratered plains outside the coronae, indeed suggesting that perhaps topography and shading have more

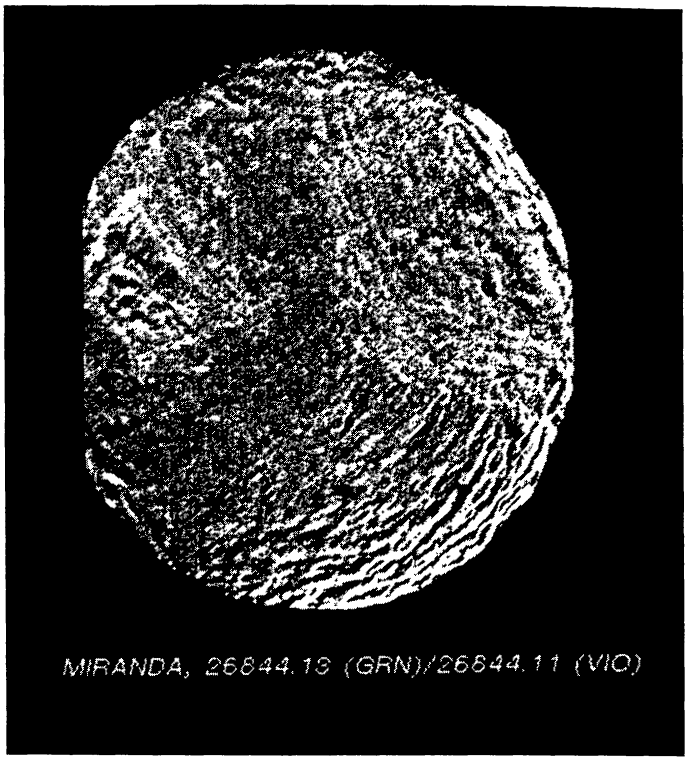


**Fig. 8.** Miranda Group 1 GRN/VIO color ratio image. The image is stretched so that black = 0.85, white = 1.05. Some of the apparent heterogeneity on Miranda seen in this image may be associated with topographic rather than compositional variations at least partially resulting from misregistration artifacts near the terminator (see text).

influence on variations between GRN/VIO images than composition on Miranda. The observed lack of substantial color heterogeneity on the same scale as the geologic diversity of Miranda is surprising but is in agreement with the more in-depth analysis of *Hillier et al.* (1989). In addition, we confirm the observation by these authors that Miranda's lower albedo regions are 3-4% redder than the surrounding terrain.

### 5.2. Ariel

Like Miranda, the Ariel ratio image shows misregistration artifacts near the rough terminator. The darkest regions in Fig. 10a are associated with craters near the lower limb and have GRN/VIO = 0.89 ± 0.07, while the majority of the heavily cratered terrain has GRN/VIO = 1.00 ± 0.04. Thus, these prominent craters along the lower limb appear less red than the rest of Ariel, but other variations associated with smooth-floored scarps and possible extrusive flows are absent. Perhaps the most obvious place to see such variations would be the floor of Sylph Chasma (labeled D in Fig. 4b); however, its GRN/VIO color ratio of 0.99 ± 0.05 is nearly identical to that of the surrounding cratered terrain. Color ratio images from Group 3 image data (Table 1) shown in Fig. 10b support the observation that the bright ejecta blankets of the craters Laica and Melusine (labeled C and B in Fig. 4b) are bluer than the surrounding terrain (viz. the BLU/VIO ratio image). In addition, the long, arcing trace of the Kachina Chasmata valley system can be seen near the top of the CLR image in Fig. 10b. There is some evidence in the accompanying color ratio images that this region is spectrally heterogeneous, although the role of shadowing at this spatial scale is difficult to quantify.

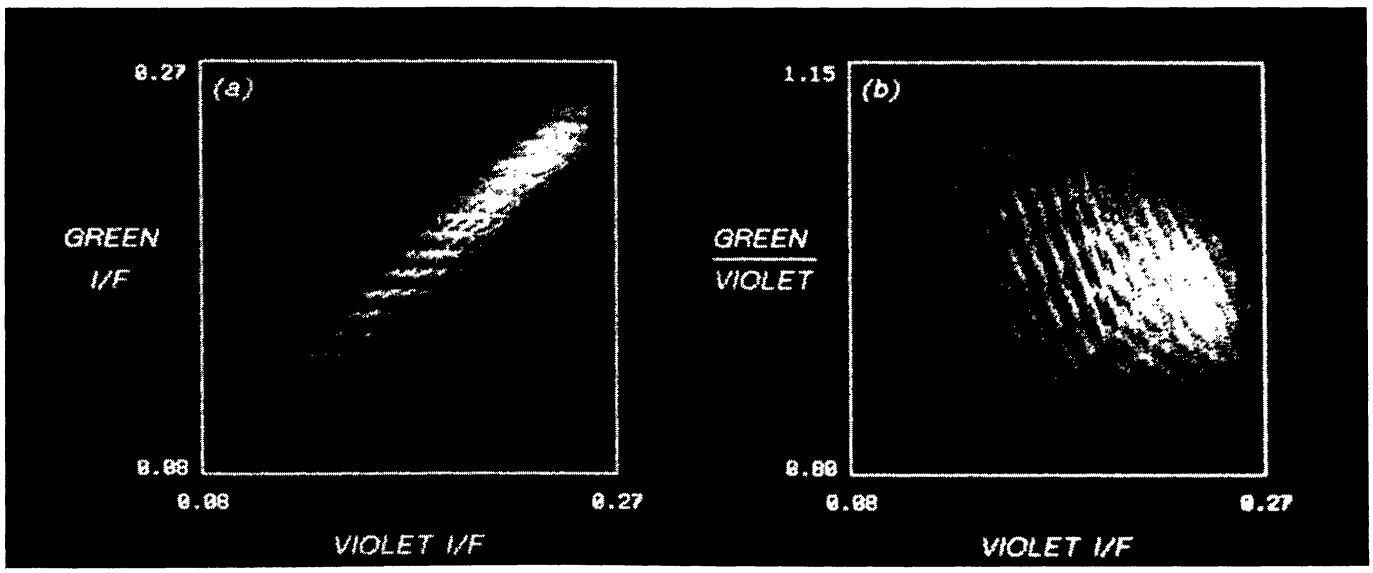


**Fig. 9.** **(a)** Two-dimensional histogram data of the Miranda GRN/VIO ratio presented in Fig. 8. The reflectance is highly correlated between these two bands, and there is little or no evidence for distinct spectral "units." Apparent "striping" in the data is a quantization effect caused by the low dynamic range of the original eight-bit Voyager data. **(b)** Two-dimensional histogram plotting Miranda GRN/VIO ratio vs. VIO reflectance. The major correlation trend (85%) seen in **(a)** has been removed, yet the data cloud is still rather compact. Subtle variations in color can be seen between bright and intermediate materials, however.

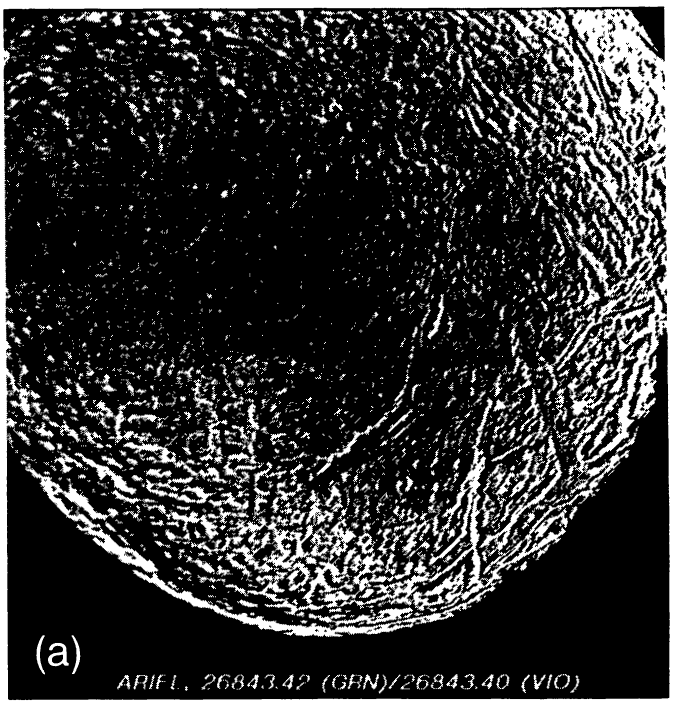


**Fig. 10.** **(a)** Ariel Group 1 GRN/VIO color ratio image. Stretch: black = 0.85, white = 1.25. Like Miranda, much of the apparent variability in this image is associated with inadequate registration of rough terminator topography. Impact craters along the limb show the most heterogeneity. **(b)** Ariel Group 2 color ratio images. Although the spatial resolution is poorer, scarps and impact crater ejecta deposits can still be identified in these images. The ratio images (especially BLU/VIO) show that these bright terrains are less red than their surroundings.

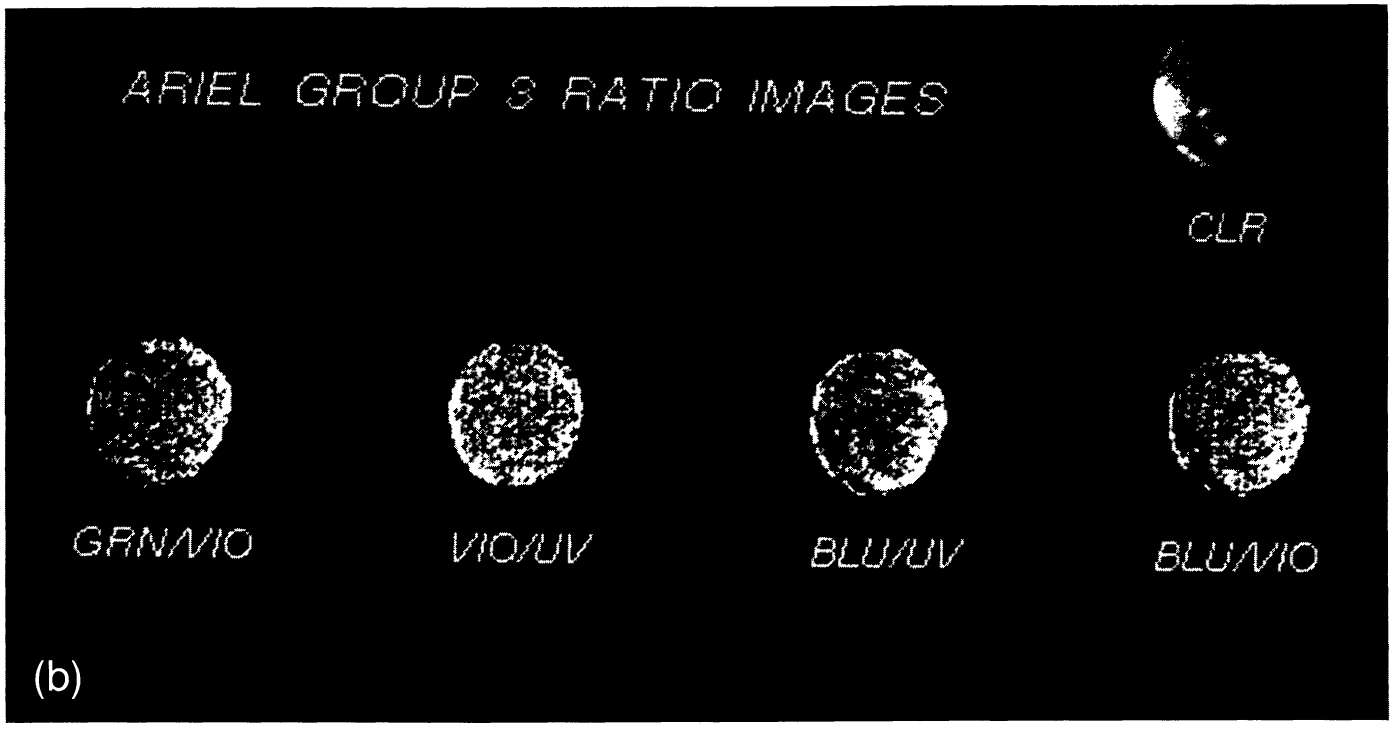


### 5.3. Umbriel

Umbriel has a remarkably uniform GRN/VIO = 0.90 ± 0.08 (Fig. 11) except for a reseau mark (artifact) along the left limb and a very small, low ratio arc associated with the bright annulus around the crater Vuver (labeled B in Fig. 5b) that has GRN/VIO = 0.835 ± 0.160. Statistics are poor for Umbriel, but the observation that the bright crater floor deposits are less red than the surrounding, supposedly older terrain is consistent with several of the other satellites. We searched the region south of Vuver for evidence of color variability associated with the global pattern of dark polygonal terrains discovered by *Helfenstein et al.* (1989b). Our results show that this region is 1-2% less red than the surrounding plains (GRN/VIO = 0.89 ± 0.17); however, the large error on this measurement makes interpretations difficult. The absence of large color variability associated with these dark polygonal terrains is most likely due to their extremely low contrast (only ≈2-3%) and the poor S/N of the Umbriel color data. Alternatively, it may indicate a situation analogous to Miranda: These albedo variations may not be associated with any measurable color change (at least at these wavelengths).

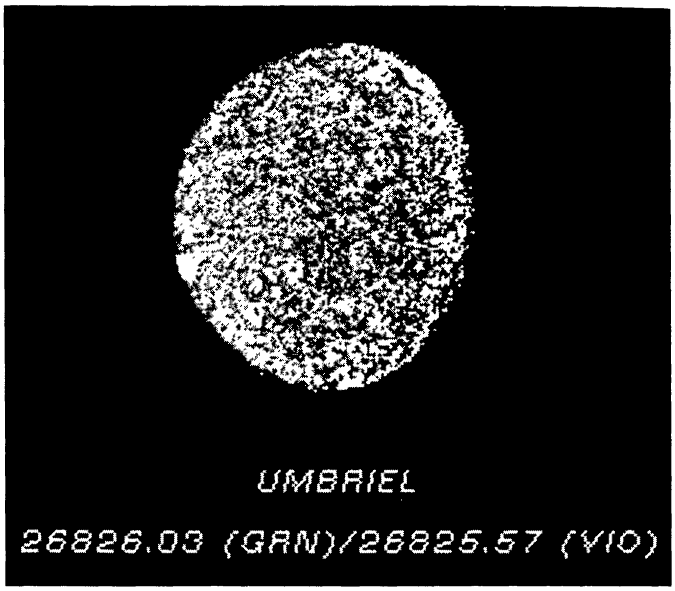


**Fig. 11.** Umbriel Group 1 GRN/VIO color ratio image. Stretch: black = 0.6, white = 1.15. The Umbriel data suffer from poor S/N, yet a dark (less red) annulus associated with the crater Vuver (labeled B in Fig. 5b) can be distinguished from an otherwise uniformly speckled background of heavily cratered terrain. The feature just below the center of the limb is a reseau artifact.

### 5.4. Titania

Several color ratios of Titania are shown in Fig. 12 for Group 1 and 2 data. Bright crater deposits [such as those marked (A) south of Ursula Crater and Jessica Crater (B) in Fig. 6b] typically show lower values of GRN/VIO ($1.01 \pm 0.06$ to $1.03 \pm 0.09$) than either the heavily cratered terrain (GRN/VIO = $1.04 \pm 0.06$) or the bright scarps [Messina Chasmata (C) in Fig. 6b; GRN/VIO = $1.12 \pm 0.13$ to $1.23 \pm 0.23$]. The high ratio and error values associated with the scarps, however, may be related to misregistration and/or shadow offsets along the terminator. Where misregistration is not a concern, the "less red" component may be caused by the exposure of more "rock" than water-ice in the craters and scarps, where the term "rock" refers simply to the non-water-ice component that does not have a flat spectrum across the visible (viz. *Hillier et al.,* 1989; *Helfenstein et al.,* 1989a). Additionally, the smooth, dark plains along the leading hemisphere mapped in Fig. 6b are 5-6% redder than the higher albedo cratered terrain and 7-8% redder than the craters themselves in both Group 1 and 2 GRN/VIO ratios. This observation may relate to variations in compaction observed by *Thomas et al.* (1987) associated with bright, cratered terrains. Alternatively, this observation may be a manifestation of a leading/trailing color and albedo asymmetry similar to that of Oberon (*Helfenstein et al.,* 1990a,b, discussed below). The UV ratio images in Fig. 12b provide some confirmation of this observation, although misregistration and smear are apparent. Of course, it is always possible with incomplete global coverage that this observation may simply indicate the fortuitous occurrence of a more reddish unit along this portion of the leading hemisphere. More rigorous image registration and mapping efforts may help.

### 5.5. Oberon

Oberon shows the most detail in the GRN/VIO ratio of all the satellites (*Helfenstein et al.,* 1989a), and the dark regions in the ratio (Fig. 13; GRN/VIO = $1.03 \pm 0.05$) directly correlate with bright crater and ejecta blanket deposits as mapped in Fig. 7b. The brighter areas in this ratio that correspond to crater floor deposits and the heavily cratered terrain have GRN/VIO = $1.07 \pm 0.06$ to $1.15 \pm 0.10$ and are thus significantly redder than the bright crater and ejecta blanket deposits. This trend is also evident in the two-dimensional GRN vs. VIO and GRN/VIO vs. VIO histograms of Fig. 14 (*Bell,* 1990). In addition, we confirm the existence of a global color asymmetry discovered by *Helfenstein et al.* (1990a): The trailing hemisphere (upper left in Group 1 images) contains a much greater fraction of more neutral color materials (GRN/VIO = $1.05 \pm 0.06$) than the more reddish (GRN/VIO = $1.15 \pm 0.10$) leading hemisphere, though the trailing hemisphere plains materials do not appear to be as "blue" as the bright crater, ejecta, and ray deposits, which can exhibit ratios as low as GRN/VIO = $0.92 \pm 0.06$ to $0.95 \pm 0.06$. The materials in the floor of Hamlet Crater (near center of Figs. 7 and 13) and Othello Crater (labeled A in Fig. 7b) exhibit some of the lowest normal albedos of any terrain on any of the satellites ($r_n \approx 0.15$; *Helfenstein et al.,* 1989a), yet their color (GRN/VIO = $1.085 \pm 0.070$) is surprisingly similar to much of the intermediate albedo heavily cratered terrain (GRN/VIO = $1.07 \pm 0.06$).

## 6. DISCUSSION

The uranian satellites are geologically diverse, but their spectral differences are subtle and generally associated with impact craters. In this study we have attempted to determine to what level geologic diversity correlates with color variability on the satellites' surfaces. Our definition of "geologic diversity" was divided into two classes: endogenic processes such as volcanism and tectonism, and exogenic processes such as impact cratering or "space weathering." Using the units defined by *Smith et al.* (1986) as a starting point, we have identified those regions on the satellites where such geologic diversity could be expected to lead to significant color heterogeneity (Figs. 3-7). Our findings indicate that there is little if any spectral variability (outside of albedo changes) associated with any of the outwardly evident endogenic features on these satellites. Nearly all the color variability detected in our study is associated with impact craters and their extended ejecta blankets.

There are several possible explanations for this observation. The first concerns two classes of very low albedo ($\leq 0.06$) solid substances of either neutral or reddish color commonly called the "dark matter" or "dark component." Many small bodies in the solar system, including planetary satellites, comets, rings, and asteroids have been found to have surfaces composed of, at least in part, a dark component that can be represented by

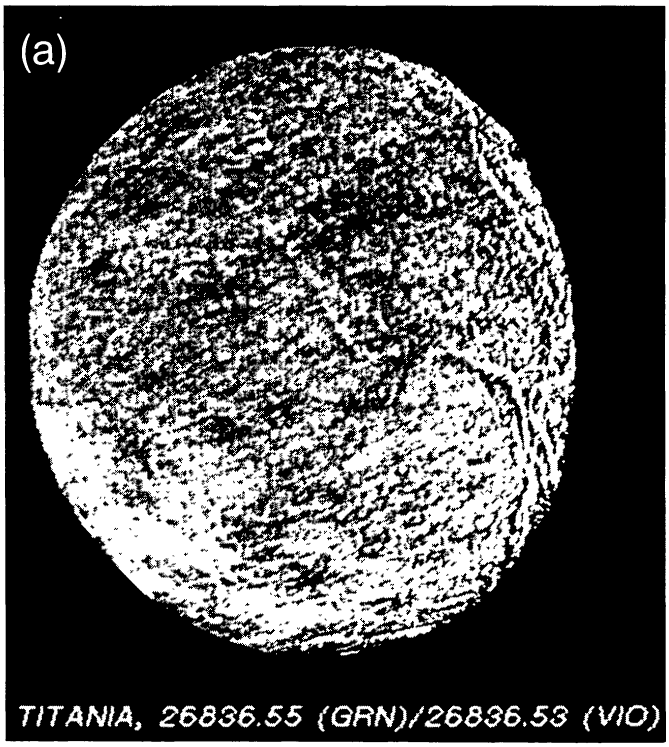


**Fig. 12.** **(a)** Titania Group 1 GRN/VIO color ratio image. Stretch: black = 0.9, white = 1.25. Spatially contiguous regions of low GRN/VIO ratio in this image are directly associated with impact craters and ejecta as mapped in Fig. 6b. In addition, the "Smooth, Dark Cratered Plains" unit in Fig. 6b is significantly redder than the heavily cratered terrain (by up to 8%) and its extent and distribution (near the central longitude of the leading hemisphere) may indicate a hemispherical color asymmetry. **(b)** Titania Group 2 color ratio images. The GRN/VIO image again shows evidence for a leading/trailing side color asymmetry (the leading hemisphere central longitude is near 12:00 in these images). Apparent difficulty with UV filter smear and misregistration hampers further support of this hypothesis, however.

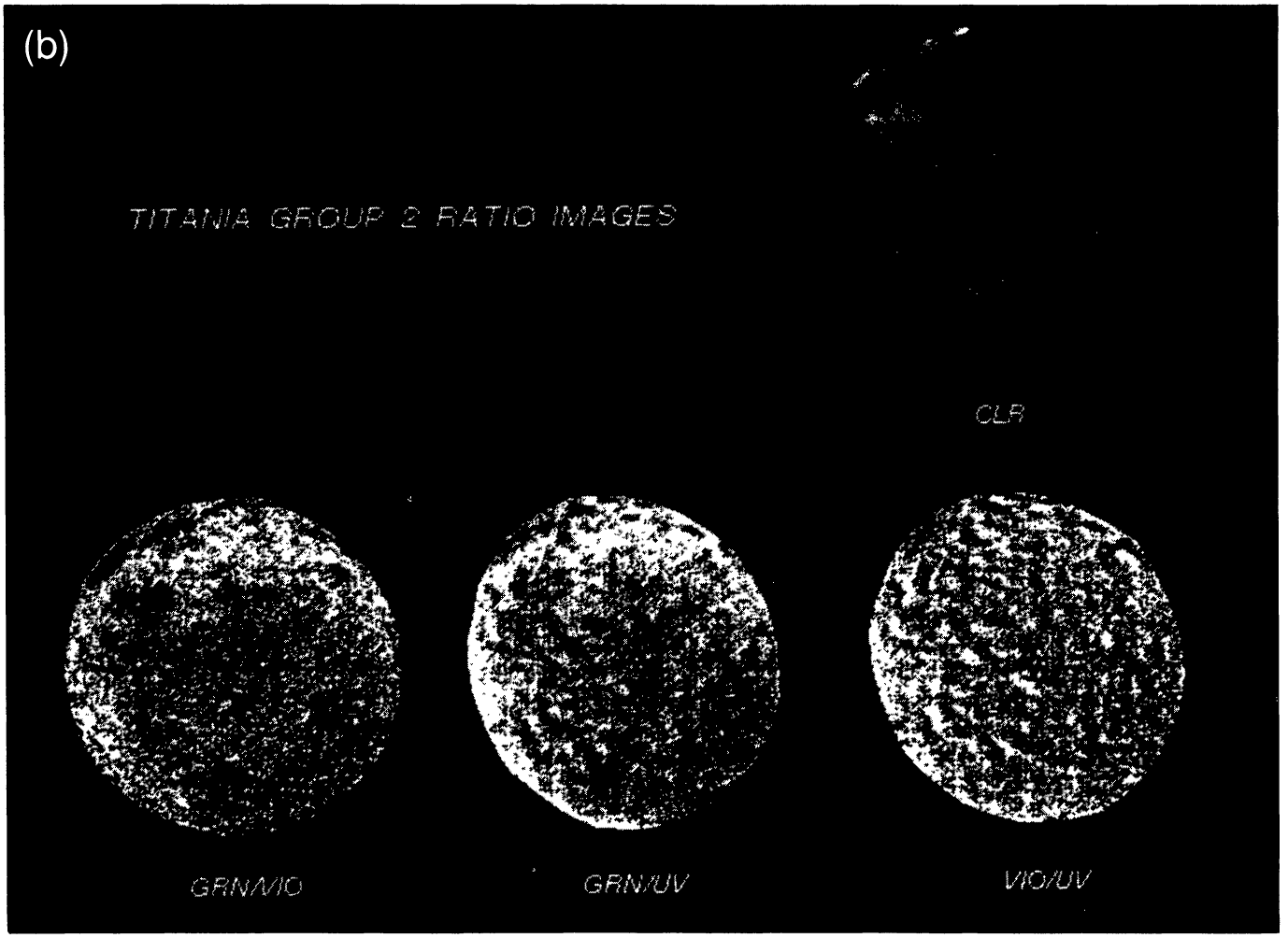

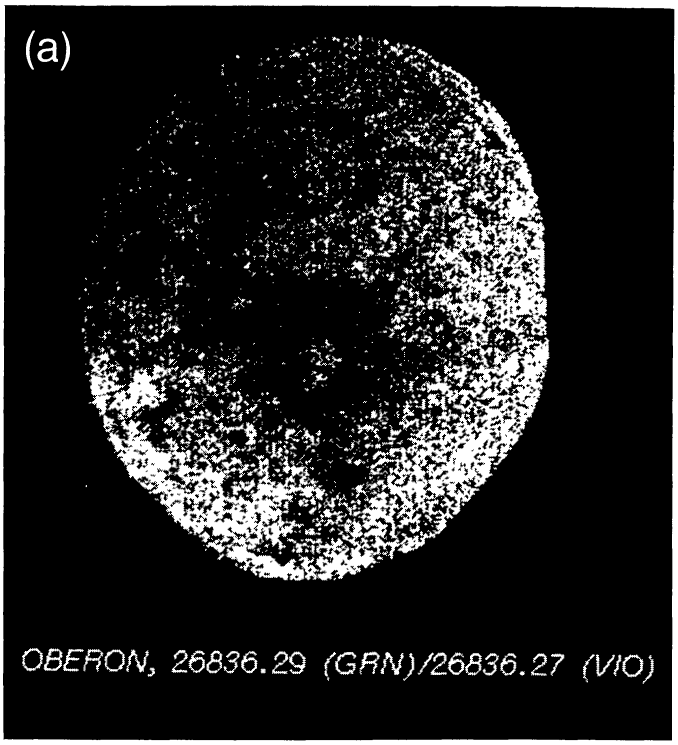


**Fig. 13.** **(a)** Oberon Group 1 GRN/VIO color ratio image. Stretch: black = 0.97, white = 1.45. Oberon shows the most color variability among all the satellites, with the low-ratio, spectrally neutral materials corresponding to the bright, extensive impact crater and ejecta deposits mapped in Fig. 7b. As well, this image confirms the discovery by *Helfenstein et al.* (1990) of a leading/trailing color asymmetry (the leading hemisphere central longitude is near 11:00). **(b)** Oberon Group 2 color ratio images. Even though the spatial resolution is poorer, the extensive ejecta blankets associated with Oberon's largest impact craters can clearly be distinguished, and the ratios presented, though exhibiting poorer S/N than Group 1 data, support the interpretations in **(a)**.

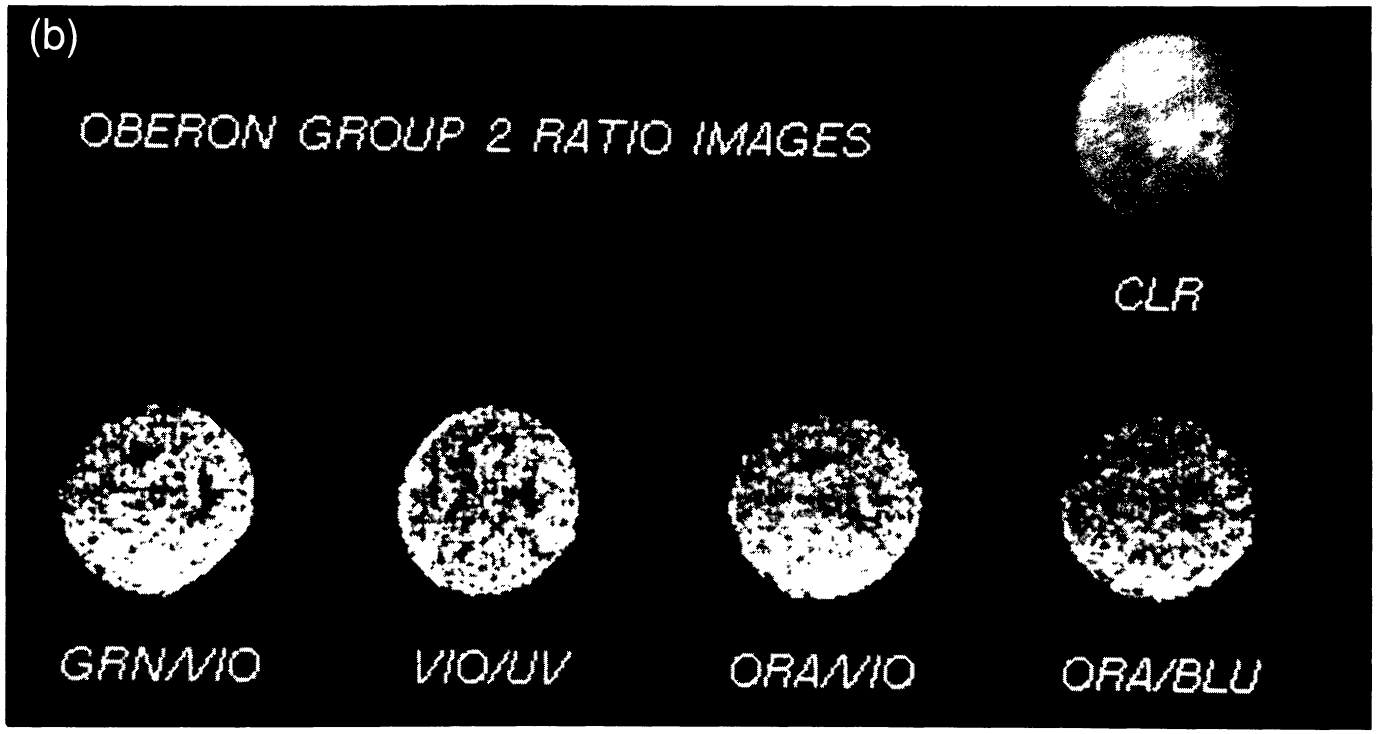


either spectrally flat, C asteroid-type materials or reddish D asteroid-type materials (e.g., *Sinton,* 1977; *Thomsen et al.,* 1978; *Cruikshank et al.,* 1983). Thus the question of determining the composition and distribution of this dark material has become one that encompasses most, if not all, aspects of outer solar system research. *Brown's* (1983) attempts to identify this dark component based on groundbased spectroscopy did not lead to unique solutions, owing mostly to the fact that sizable, distinct spectral features simply do not exist for many of the candidate materials in this wavelength range and thus their identification is speculative at best. The data of *Brown* (1983) did demonstrate that the uranian satellite spectra are reasonably matched with spectra of fine-grained water frosts and intimately mixed charcoal and water-ice;

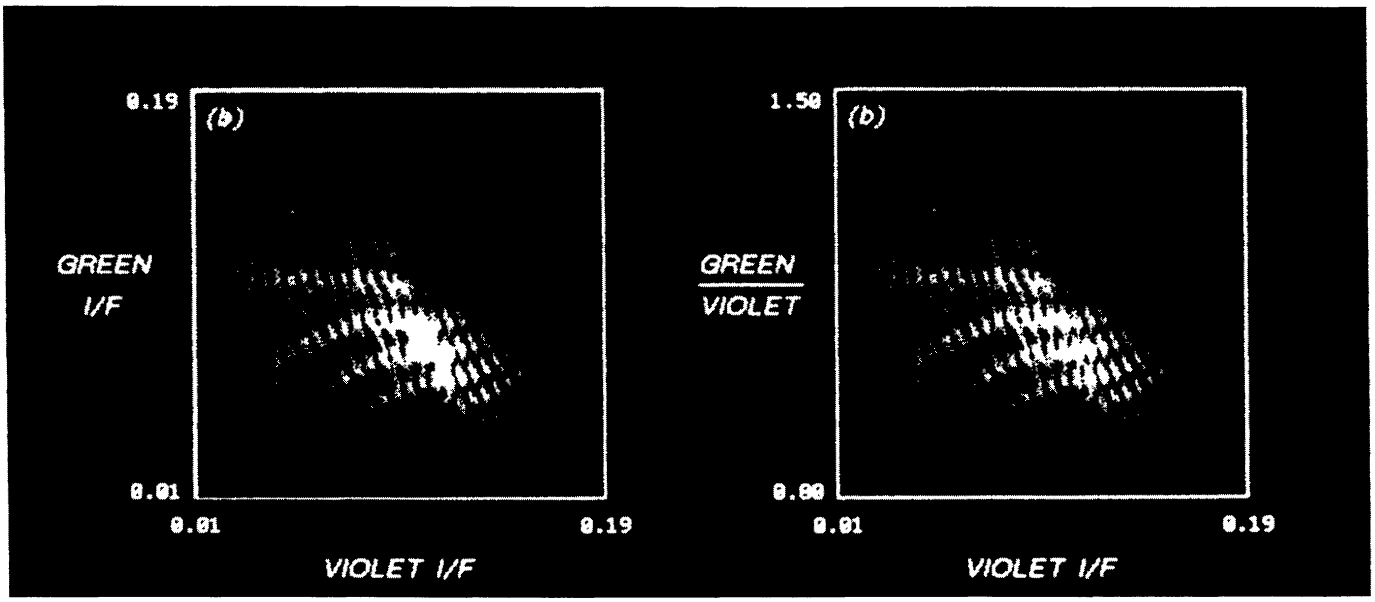


**Fig. 14.** **(a)** Two-dimensional histogram data of the Oberon GRN/VIO ratio presented in Fig. 13. Two distinct linear trends can be seen in the data: the brighter impact crater and ejecta blanket materials are less "red" (lower GRN/VIO slope) than the relatively neutral color, lower reflectance materials (dark crater floors and heavily cratered plains). **(b)** Two-dimensional histogram plotting Oberon GRN/VIO ratio vs. VIO reflectance. The major correlation trend (98%) seen in **(a)** has been removed. Variations in color can be seen between bright and intermediate materials, with the break at VIO $\approx$ 0.12 corresponding to the spectral slope change observed in **(a)**.

however, the similarities between the many different candidate dark materials (70% charcoal with 30% water-ice, carbon lampblack, Murchison organics) preclude further identification. The data do argue for the presence of carbon or carbon-rich mixtures, however, which ties in well with carbonaceous chondrite compositions and accepted solar nebula accretion models at 19 AU.

Such models of the satellite surfaces as mixtures of spectrally bland materials (differing only in albedo in the visible; *Brown,* 1983; *Hillier et al.,* 1989) are consistent with much of the color ratio data presented here, although perhaps these models underestimate the importance of the "continuum slope" spectral parameter, which may be an important variable controlling the observed color variability of the satellites. Continuum variations can arise from a combination of effects, including wavelength-dependent specular or multiple scattering, wavelength-independent absorption, and far-wing effects associated with extremely strong absorptions (e.g., *Wendlandt and Hecht,* 1966; *Clark and Roush,* 1984). This latter effect is most often associated with UV charge transfer absorptions, and it is not unusual for charge transfer absorption wings to extend well into the visible (e.g., *Burns,* 1970). Unfortunately, uncertainties in the Voyager filter calibrations (especially the UV) make it nearly impossible to reliably measure such a continuum effect in these data. Such uncertainties combined with the limited spectral range of the Voyager cameras inhibit the detectability of materials that are almost surely compositionally different.

A second possible explanation for the observation of little color variability associated with endogenic features is that volcanic/tectonic processes on the satellites are erupting or exposing materials compositionally similar to the substrate. In this case it could be argued that graben floors on Ariel or Miranda's dark coronal plains should not be expected to show color heterogeneity. Some possible support for this idea comes from the observation noted here and previously by *Helfenstein et al.* (1990a,b) that dark, supposedly extrusive materials on crater floors on Oberon (*Smith et al.,* 1986) differ little in their color characteristics from much of the surrounding heavily cratered terrain. If significant compositional diversity of materials associated with endogenic processes is indeed absent, how then do the color differences associated with impact processes arise?

Possible answers to this question can be found in recent attempts to model processes at work on/in these satellite surfaces that can account for the dark matter. One theory explains that the dark component is the direct result of irradiation of methane ice exposed to intense or prolonged magnetospheric or solar wind fluxes on the surface (*Strazzulla et al.,* 1983; *Calcagno et al.,* 1985; *Thompson et al.,* 1987). Methane ices and low occupancy ratio methane clathrates have been shown by these workers in the laboratory to darken considerably under various types of irradiation; however, further laboratory work and expanded spectral coverage are needed to correlate these results to groundbased spectrophotometry, and as yet there is no compelling evidence for the existence of methane ices on the uranian satellites. Alternatively, *Helfenstein et al.* (1990a,b) have interpreted Oberon's hemispheric color and albedo asymmetry as indicating that much of Oberon's dark materials are either mare-like flood

deposits or an impact-excavated dark subsurface layer, and thus the observed leading/trailing color asymmetry is a manifestation of a global crustal thickness asymmetry.

A third possibility is that a process similar in nature to lunar vitrification darkening/reddening occurs on these satellites (e.g., *Adams and McCord,* 1971; *Matson et al.,* 1977). This assumes that a significant component of the optical surface of these satellites is composed of minerals or mineral/ice mixtures, and impact cratering and micrometeorite gardening/pulverization act over time to form greater concentrations of impact-melt glasses that alter the spectral properties of the optical surface of these minerals. On the Moon, younger, more recently disturbed impacted terrains are optically "young": They exhibit typically higher albedos and relatively gray spectra. Older, "mature" surfaces are darker and have generally redder spectra with much lower contrast absorption bands (higher glassy component). Data presented in this paper and elsewhere suggest that a similar, though weaker trend may exist for the uranian satellites. For example, Oberon's bright crater ray deposits may be analogous to "fresh" lunar crater rays in their optical (though certainly not compositional) properties. There are several problems with the application of this idea to these satellites, however. A major one is the generally poor correlation between albedo and age as determined from crater size/frequency distributions (*Plescia,* 1987; *Strom,* 1987). "Young" terrains exist on Miranda and Oberon that are both very bright and very dark relative to surrounding heavily cratered terrains. If such regions are the result of "recent" endogenic activity (i.e., mare-type volcanism in Oberon crater floors as proposed by *Smith et al.,* 1986, and *Helfenstein et al.,* 1990a,b), then the vitrification model may only apply to the oldest preserved regions on the satellites, since the timescale for optical maturation in the outer solar system is most likely a major fraction of the lifetime of these satellites. The lunar timescale for optical maturity appears to be relatively short (Copernicus is "mature"; *McCord et al.,* 1972), but the vitrification timescale is likely to be much longer at 19 AU due to a strong dependence on micrometeorite impact velocity, gravity, heliocentric distance, and composition (*Soderblom,* 1970; *Matson et al.,* 1977). The latter factor is particularly important for the uranian satellites since little is known about the composition of the dark, spectrally neutral "rock" component or the way ice-rock mixtures "mature" in the outer solar system environment. A second problem with the vitrification model is its incorporation into the observed global color asymmetries of Oberon and Titania. As mentioned above, far from complete global imaging coverage of these satellites may have led to the fortuitous occurrence of color unit boundaries along the imaged portions of their leading hemispheres. However, if these hemispheric asymmetries are real, then an additional mechanism such as preferential leading hemisphere bombardment (*Shoemaker and Wolfe,* 1982) is required in order to account for the 5-10% redder leading hemispheres of Oberon and Titania. If further research and more quantitative calculations show that the vitrification model is viable, it may indicate that endogenic tectonic/volcanic resurfacing events occurred very early in these satellites' histories, and the resulting materials extruded or exposed are presently optically mature. In this respect, the vitrification hypothesis would be consistent with recent results on the origin of endogenic terrains on Miranda and Ariel (*Smith et al.,* 1986; *Janes and Melosh,* 1988; *Jankowski and Squyres,* 1988), Oberon (*Helfenstein et al.,* 1990b) and Umbriel (*Helfenstein et al.,* 1989b).

## 7. CONCLUSIONS

1. All the uranian satellites exhibit some degree of spectral variability associated with bright impact craters, with the typical trend being that the bright craters and their associated ejecta deposits are *less red* than the remainder of the satellite by 5-30%. Oberon clearly exhibits the greatest variability of all the satellites, followed by Titania and Ariel. A number of possible mechanisms (none of them mutually exclusive) for the observed color heterogeneity exist, including an outer solar system analog to lunar vitrification darkening/reddening that causes a slow, optical "maturing" of freshly exposed surfaces, irradiation darkening of methane ices (*Thompson et al.,* 1987), or the preferential eruption or excavation of darker, redder materials in the satellites' leading hemispheres (*Helfenstein et al.,* 1990a,b).

2. Morphologic features on Miranda and Ariel possibly associated with endogenic processes such as tectonism or ice volcanism *do not* show as high a degree of spectral variability relative to their surroundings as bright impact craters. Material that has been erupted or extruded on these satellites is either the same composition as the substrate, spectrally indistinguishable in the visible, or it (and/or the substrate) has been modified by some external process so that it is now spectrally indistinct.

3. Unique compositional information cannot be obtained from the Voyager multispectral dataset, which covers only up to 25-40% of the satellites' surfaces in only 3-6 broad wavelength bands across the VIS. A higher spatial/spectral resolution mapping program (modeled after Galileo NIMS or CRAF VIMS) is required to pin down compositions and unit distributions. The uranian satellites are indeed quite gray, but this work and the studies of *Hillier et al.* (1989) and *Helfenstein et al.* (1989a, 1990a,b) have shown that at finer spatial scales these satellites exhibit subtle yet detectable spectral differences.

***Acknowledgments.*** The authors thank M. Robinson, A. McEwen, S. Willis, and D. Nitsch for data reduction and calibration assistance. In addition, we are grateful to P. Helfenstein and an anonymous reviewer for very helpful reviews and discussion. This work was supported by NASA UDAP grant NAGW-1492. This paper is Planetary Geosciences Division Contribution No. 599.

## REFERENCES

Adams J. B. and McCord T. B. (1971) Alteration of lunar optical properties: Age and composition effects. *Science, 171,* 567-571.

Bell J. F. III (1990) Color units on the Uranian satellites: An outer solar system analog to lunar vitrification darkening? (abstract). In *Lunar and Planetary Science XXI,* pp. 58-59. Lunar and Planetary Institute, Houston.

Bell J. F., Clark R. N., McCord T. B., and Cruikshank D. P. (1979) Reflection spectra of Pluto and three distant satellites (abstract). *Bull. Am. Astron. Soc., 11,* 570.

Brown R. H. (1983) The Uranian satellites and Hyperion: new spectrophotometry and compositional implications. *Icarus, 56,* 414-425.

Brown R. H. and Clark R. N. (1984) Surface of Miranda: identification of water ice. *Icarus, 58,* 288-292.

Buratti B., Wong F., and Mosher J. (1990) Surface properties and photometry of the Uranian satellites. *Icarus, 84,* 203-214.

Burns R. G. (1970) *Mineralogical Applications of Crystal Field Theory.* Cambridge Univ., New York. 224 pp.

Calcagno L., Foti G., Torrisis L., and Strazzulla G. (1985) Fluffy layers obtained by ion bombardment of frozen methane: experiments and applications to Saturnian and Uranian satellites. *Icarus, 63,* 31-38.

Clark R. N. and Roush T. L. (1984) Reflectance spectroscopy: Quantitative analysis techniques for remote sensing applications. *J. Geophys. Res., 89,* 6329-6240.

Croft S. K. (1987) Miranda geology and tectonics: a non-catastrophic interpretation (abstract). In *Lunar and Planetary Science XVIII,* pp. 207-208. Lunar and Planetary Institute, Houston.

Croft S. K. and Soderblom L. A. (1990) Geology of the Uranian satellites. In *Uranus* (J. Bergstralh and E. Minor, eds.). Univ. of Arizona, Tucson, in press.

Cruikshank D. P. (1980) Near-infrared studies of the satellites of Saturn and Uranus. *Icarus, 41,* 246-258.

Cruikshank D. P. and Brown R. H. (1981) The Uranian satellites: water ice on Ariel and Umbriel. *Icarus, 45,* 607-611.

Cruikshank D. P., Bell J. F., Gaffey M. J., Brown R. H., Howell R., Beerman C., and Rognstad M. (1983) The dark side of Iapetus. *Icarus, 53,* 90-104.

Danielson G. E., Kupferman P., Johnson T., and Soderblom L. (1981) Radiometric performance of the Voyager cameras. *J. Geophys. Res., 86,* 8583-8689.

Davies M., Corvin T. R., Katayama F. Y., and Thomas P. C. (1987) The control network of the satellites of Uranus. *Icarus, 71,* 137-147.

Harris D. L. (1961) Photometry and colorimetry of planets and satellites. In *Planets and Satellites* (G. P. Kuiper and B. M. Middlehurst, eds.), pp. 272-342. Univ. of Chicago, Chicago.

Helfenstein P., Veverka J., and Thomas P. C. (1988) Uranus satellites: Hapke parameters from Voyager disk-integrated photometry. *Icarus, 74,* 231-239.

Helfenstein P., Hillier J., Veverka J., Moersch J., and Weitz C. (1989a) Uranus satellites: Albedo and color maps from Voyager imaging (abstract). In *Lunar and Planetary Science XX,* pp. 402-403. Lunar and Planetary Institute, Houston.

Helfenstein P., Thomas P. C., and Veverka J. (1989b) Evidence from Voyager II photometry for early resurfacing of Umbriel. *Nature, 338,* 324-326.

Helfenstein P., Hillier J., Weitz C., and Veverka J. (1990a) Oberon: Color photometry and its geological implications (abstract). In *Lunar and Planetary Science XXI,* pp. 489-490. Lunar and Planetary Institute, Houston.

Helfenstein P., Hillier J., Weitz C., and Veverka J. (1990b) Oberon: Color photometry from Voyager and its geological implications. *Icarus,* in press.

Hillier J., Helfenstein P., and Veverka J. (1989) Miranda: Color and albedo variations from Voyager photometry. *Icarus, 82,* 314-355.

Janes D. M. and Melosh H. J. (1988) Sinker tectonics: An approach to the surface of Miranda. *J. Geophys. Res., 93,* 3127-3143.

Jankowski D. G. and Squyres S. W. (1988) Solid-state ice volcanism on the satellites of Uranus. *Science, 241,* 1322-1325.

Johnson P. E., Greene T. F., and Shorthill R. W. (1978) Narrow-band spectrophotometry of Ariel, Umbriel, Oberon, and Triton. *Icarus, 36,* 75-81.

Johnson T. V., Brown R. H., and Pollack J. B. (1987) Uranus satellites: Densities and composition. *J. Geophys. Res., 92,* 14884-14894.

Matson D. L., Johnson T. V., and Veeder G. J. (1977) Soil maturity and planetary regoliths: The Moon, Mercury, and the asteroids. *Proc. Lunar Sci. Conf. 8th,* pp. 1001-1011.

McCord T. B., Charette M. P., Johnson T. V., Lebofsky L. A., and Pieters C. (1972) Lunar spectral types. *J. Geophys. Res., 77,* 1349-1359.

Plescia J. B. (1987) Cratering history of the Uranian satellites: Umbriel, Titania, and Oberon. *J. Geophys. Res., 92,* 14918-14932.

Reitsema H. J., Smith B. A., and Weistrop D. E. (1978) Visual and near-infrared photometry of the Uranian satellites (abstract). *Bull. Am. Astron. Soc., 10,* 585.

Shoemaker E. M. and Wolfe R. F. (1982) Cratering timescales for the Galilean satellites. In *Satellites of Jupiter* (D. Morrison, ed.), pp. 277-339. Univ. of Arizona, Tucson.

Sinton W. M. (1977) Uranus: the rings are black. *Science, 198,* 503-504.

Smith B. A., Soderblom L. A., Batson R., Bridges P., Inge J., Masursky H., Shoemaker E. M., Beebe R., Boyce J., Briggs G. A., Bunker A., Collins S. A., Hansen C. J., Johnson T. V., Mitchell J. L., Terrile R. J., Cook A. F. II, Cuzzi J. N., Pollack J. B., Danielson G. E., Morrison D., Owen T., Sagan C., Veverka J., Strom R. G., and Suomi V. E. (1982) A new look at the Saturnian system: The Voyager 2 images. *Science, 215,* 504-537.

Smith B. A., Soderblom L. A., Beebe R., Bliss D., Boyce J. M., Brahic A., Briggs G. A., Brown R. H., Collins S. A., Cook A. F. II, Croft S. K., Cuzzi J. N., Danielson G. E., Davies M. E., Dowling T. E., Godfrey D., Hansen C. J., Harris C., Hunt G. E., Ingersoll A. P., Johnson T. V., Krauss R. J., Masursky H., Morrison D., Owen T., Plescia J. B., Pollack J. B., Porco C. C., Rages K., Sagan C., Shoemaker E. M., Sromovsky L. A., Stoker C., Strom R. G., Suomi V. E., Synnott S. P., Terrile R. J., Thomas P., Thompson W. R., and Veverka J. (1986) Voyager 2 in the Uranian system: Imaging science results. *Science, 233,* 43-64.

Soderblom L. A. (1970) A model for small-impact erosion applied to the lunar surface. *J. Geophys. Res., 75,* 2655-2661.

Soifer B. T., Neugebauer G., and Matthews K. (1981) Near-infrared spectrophotometry of the satellites and rings of Uranus. *Icarus, 45,* 612-617.

Strazzulla G., Calcagno L., and Foti G. (1983) Polymerization induced on interstellar grains by low-energy cosmic rays. *Mon. Not. R. Astron. Soc., 204,* 59-62.

Strom R. G. (1987) The solar system cratering record: Voyager 2 results at Uranus and implications for the origin of impacting objects. *Icarus, 70,* 517-535.

Thomas P. C., Veverka J., Helfenstein P., Brown R. H., and Johnson T. V. (1987) Titania's opposition effect: Analysis of Voyager observations. *J. Geophys. Res., 92,* 14911-14917.

Thompson W. R., Murray B. G. J. P. T., Khare B. N., and Sagan C. (1987) Coloration and darkening of methane clathrate and other ices by charged particle irradiation: Applications to the outer solar system. *J. Geophys. Res., 92,* 14933-14948.

Thomsen B., Baum W. A., Wilkensen D. T., and Loh E. H. (1978) New results on the albedo of the rings around Uranus (abstract). *Bull. Am. Astron. Soc., 10,* 581-582.

Veverka J., Thomas P., Helfenstein P., Brown R. H., and Johnson T. V. (1987) Satellites of Uranus: Disk-integrated photometry from Voyager imaging observations. *J. Geophys. Res., 92,* 14895-14904.

Veverka J., Helfenstein P., Skypeck A., and Thomas P. (1989) Minnaert photometric parameters for the satellites of Uranus. *Icarus, 78,* 14-26.

Wendlandt W. W. and Hecht H. G. (1966) *Reflectance Spectroscopy.* Wiley, New York. 298 pp.